



# LiF by atomic layer deposition—Made easy

Cite as: J. Vac. Sci. Technol. A **38**, 050401 (2020); <https://doi.org/10.1116/6.0000314>

Submitted: 08 May 2020 . Accepted: 17 July 2020 . Published Online: 06 August 2020

 Julie N. Kvalvik,  Kristian B. Kvamme,  Kjetil Almaas,  Amund Ruud,  Henrik H. Sønsteby, and  Ola Nilsen



View Online



Export Citation



CrossMark

## ARTICLES YOU MAY BE INTERESTED IN

### Consistency and reproducibility in atomic layer deposition

Journal of Vacuum Science & Technology A **38**, 020804 (2020); <https://doi.org/10.1116/1.5140603>

### tert-butoxides as precursors for atomic layer deposition of alkali metal containing thin films

Journal of Vacuum Science & Technology A **38**, 060804 (2020); <https://doi.org/10.1116/6.0000589>

### Understanding chemical and physical mechanisms in atomic layer deposition

The Journal of Chemical Physics **152**, 040902 (2020); <https://doi.org/10.1063/1.5133390>



Advance your science and  
career as a member of

AVS

LEARN MORE




# LiF by atomic layer deposition—Made easy

Cite as: J. Vac. Sci. Technol. A 38, 050401 (2020); doi: 10.1116/6.0000314

Submitted: 8 May 2020 · Accepted: 17 July 2020 ·

Published Online: 6 August 2020



Julie N. Kvalvik,<sup>1</sup>  Kristian B. Kvamme,<sup>1</sup> Kjetil Almaas,<sup>1</sup> Amund Ruud,<sup>1,2</sup>  Henrik H. Sønsteby,<sup>2</sup>   
and Ola Nilsen<sup>1,a)</sup> 

## AFFILIATIONS

<sup>1</sup>Department of Chemistry, Centre for Materials Science and Nanotechnology, University of Oslo, Sem Sælandsvei 26, Oslo 0371, Norway

<sup>2</sup>Nordic Institute of Dental Materials, Sognsveien 70 A, Oslo 0855, Norway

<sup>a)</sup>Electronic mail: [ola.nilsen@kjemi.uio.no](mailto:ola.nilsen@kjemi.uio.no)

## ABSTRACT

Lithium fluoride (LiF) is an integral part of UV optics. Recently, it has also gained attention for its role in the solid-electrolyte interphase on the anode of lithium-ion batteries. Atomic layer deposition (ALD) is the preferred tool for synthesizing conformal and pin-hole free LiF thin films, especially on high aspect ratio structures. Present routes to deposit LiF by ALD are based on HF or HF-pyridine as the fluorine source, requiring strict safety precautions. Other routes involve TiF<sub>4</sub> or WF<sub>6</sub>, resulting in inclusions of Ti or W impurities in the resulting films. Herein, we present a new route to deposit LiF by ALD, using lithium *tert*-butoxide (LiO<sup>t</sup>Bu) and NH<sub>4</sub>F as precursors. The process yields uniform films over a broad temperature range (150–300 °C), with a growth per cycle of 50.9 pm/cycle (225 °C). The films are free from any nitrogen contamination from the NH<sub>4</sub>F precursor. This process provides a facile route for high purity LiF thin films with the use of less harmful precursor chemistry.

Published under license by AVS. <https://doi.org/10.1116/6.0000314>

## I. INTRODUCTION

Lithium fluoride (LiF) is a large bandgap material with applications within bulk heterojunction polymers<sup>1–3</sup> and perovskite photovoltaics,<sup>4–6</sup> and is found in the solid electrolyte interphase (SEI) in lithium-ion batteries.<sup>7</sup> A strategy to enhance battery performance is to preform, and thus control, SEIs.<sup>8</sup> Preforming LiF coatings as artificial SEIs has been shown to reduce Mn-dissolution in manganite based cathodes and improve cycling stability on both lithium metal and silicon anodes.<sup>9</sup> Among a range of viable techniques for the deposition of LiF, atomic layer deposition (ALD) excels as an ideal method for coating uniform, thin, and pinhole-free LiF films for batteries and optics. ALD also provides the possibility of conformal coatings of high aspect ratio substrates, an essential feature for fabricating devices such as 3D batteries.<sup>10–14</sup> ALD is already in use in the kiloton scale within the battery<sup>15</sup> and solar industries,<sup>16</sup> although for the deposition of various oxides, such as Al<sub>2</sub>O<sub>3</sub>. A handful of routes for deposition of LiF by ALD has been reported and summarized in Table I.

Using LiO<sup>t</sup>Bu and hexafluoroacetylacetone was also attempted recently, but this yielded porous LiF-CF<sub>x</sub> hybrid films.<sup>9</sup> Several of the established routes use either HF or HF-pyridine as the fluorine

source, requiring strict safety precautions. Moreover, using TiF<sub>4</sub> or WF<sub>6</sub> as the fluorine source leads to traces of Ti or W in the resulting films. Here, we extend the toolbox of ALD LiF-processes by depositing phase pure, crystalline thin films, combining LiO<sup>t</sup>Bu and NH<sub>4</sub>F, which was introduced as an ALD-precursor already in 1994.<sup>17</sup>

## II. EXPERIMENT

Thin films were deposited in an F-120 Sat ALD reactor (ASM Microchemistry). LiO<sup>t</sup>Bu (Sigma Aldrich, 97%) and NH<sub>4</sub>F (Sigma Aldrich, 99.99%) were used as precursors delivered from open boats inside the reactor held at 130 and 95 °C, respectively. Pulsing/purging times were 5 s/5 s and 7 s/3 s for LiO<sup>t</sup>Bu and NH<sub>4</sub>F, respectively. Standard pulsing and purging times are used unless otherwise stated. N<sub>2</sub> was used as a purging gas, supplied from gas cylinders (Praxair, 99.999%), passing through a Mykrolis purifier and kept at a primary flow rate of 300 cm<sup>3</sup> min<sup>-1</sup>. A background pressure of 4.5 ± 1 mbar was maintained throughout all depositions. Unless otherwise stated, 1000 ALD cycles are employed for each of the depositions. The films were deposited on 1 × 1 cm<sup>2</sup> Si(100) substrates with a ~2 nm thick native oxide layer.

TABLE I. List of reported ALD-processes used to deposit LiF and their key characteristics.

Li-source	F- source	GPC (pm per cycle)	Deposition temperature (°C)	Crystal structure	Reference
LiO <sup>t</sup> Bu	HF-pyridine	88 at 150 °C	150	Rock salt	22
LiHMDS	HF-pyridine	58 at 150 °C	125–250	Rock salt	18
Li(thd)	TiF <sub>4</sub>	148 at 250 °C	250–350	Rock salt	24
LiHMDS	Anhydrous HF	150 at 150 °C	100–250	n/a	25
LiO <sup>t</sup> Bu	WF <sub>6</sub>	n/a	150–300	n/a	26
LiO <sup>t</sup> Bu	MoF <sub>6</sub>	260 at 150 °C	150–300	Rock salt above 150 °C	26
LiO <sup>t</sup> Bu	TiF <sub>4</sub>	50 at 250 °C	200–300	Rock salt	9,27
LiO <sup>t</sup> Bu	Hhfac	n/a	220	n/a	9
LiO <sup>t</sup> Bu	NH <sub>4</sub> F	55 at 250 °C	150–300	Rock salt	This work

The substrates were cleaned with ethanol and blown dry with pressurized air prior to deposition. Growth dynamics were measured *in situ* at 225 °C by a quartz crystal microbalance (QCM) using an Eon-LT monitor (Colnatec) and a self-made crystal holder. An AT-cut gold-plated quartz crystal (Inficon SPC-1157-G1) with a 6 MHz nominal frequency was used. The presented QCM data show an average over 16 consecutive ALD cycles for improved statistics. The density of a LiF film was measured *ex situ* by x-ray reflectivity (XRR), with the extracted density and thickness used for converting the response of the QCM crystal to mass gain per unit area of the film. A known LiF deposition sequence was added several places in the QCM campaign as an internal standard to accommodate for variations in surface texture, and thus evolution of surface area of the QCM crystal during the campaign. A PANalytical Empyrean diffractometer with a CuK $\alpha$  source, a parallel beam mirror with a 1/32° divergence slit, a 0.27° parallel plate collimator, 0.04 rad soller slits, and an automatic nickel attenuator was used for the XRR measurements. The XRR data were modeled and analyzed using the accompanying X'Pert Reflectivity software. The thickness and refractive indices at  $\lambda = 632.8$  nm for the thin films were investigated with spectroscopic ellipsometry using an alpha-SE (J.A. Woollam). The collected SE data were fitted successfully with a Cauchy model using the CompleteEASE software.

LiF thin films were characterized with respect to composition, crystal structure, and morphology. X-ray spectroscopy (XPS) was performed with a Thermo Scientific Theta Probe Angle-Resolved XPS system, equipped with a standard Al K $\alpha$  source ( $h\nu = 1486.6$  eV). Pass-energies of 200 and 60 eV were employed for survey scans and detailed scans, respectively. The resulting data were treated using the Thermo Scientific Avantage software suite. X-ray diffraction (XRD) was carried out to investigate the crystal structure of the obtained samples, using a Bruker D8 Discovery Diffractometer, with a CuK $\alpha$  source and a Ge(111) monochromator in a traditional Bragg-Brentano geometry.

Selected samples were measured by synchrotron XRD at BM01 at ESRF (Grenoble, France) for mapping a large portion of the reciprocal space and characterizing the angular scattering distribution of the LiF crystallites. The beamline employed a wavelength of 0.697 05 Å, and a Dectris Pilatus 2 M detector. Morphology was investigated using a Park Systems XE-70 atomic force microscope (AFM) with a CONTSCR tip in contact mode. It was further

investigated by a HITACHI SU 8230 scanning electron microscope (SEM) with a cold cathode field emission gun using an acceleration voltage of 5.0 kV, a beam current of 5  $\mu$ A, and a working distance of 3.3 mm.

### III. RESULTS AND DISCUSSION

The first step when establishing the LiO<sup>t</sup>Bu + NH<sub>4</sub>F process for the deposition of LiF by ALD, was to perform an *in situ* QCM experiment to determine if the process is ALD compatible (i.e., exhibiting saturative growth). The experiment was also used to determine the mass gain per cycle, Fig. 1, and appropriate pulsing and purging parameters, Fig. 2. Net mass gain per cycle was 10.5 ng/cm<sup>2</sup> with a mass gain of 34.0 ng/cm<sup>2</sup> during the LiO<sup>t</sup>Bu pulse and a mass loss of 23.5 ng/cm<sup>2</sup> during the NH<sub>4</sub>F pulse.

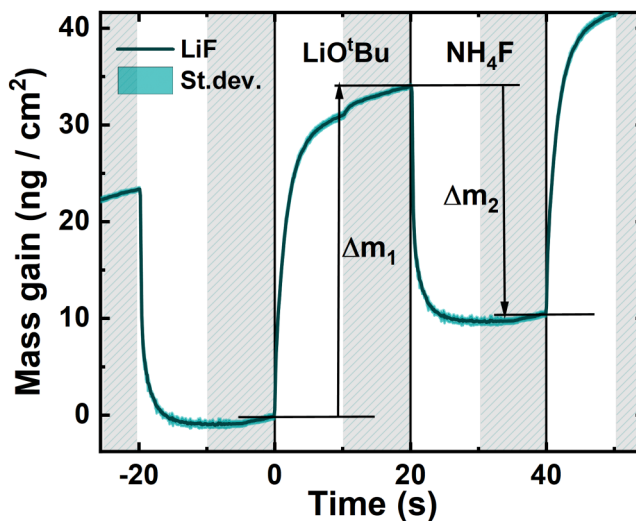


FIG. 1. Mass variation (ng/cm<sup>2</sup>) during one cycle of LiO<sup>t</sup>Bu and NH<sub>4</sub>F at 225 °C as measured by *in situ* QCM. The QCM crystal was placed in the front of the reaction chamber. The green area denotes the standard deviation of the average of 16 cycles. Light gray shaded areas correspond to the inert gas purging steps. All pulses and purges were 10 s.

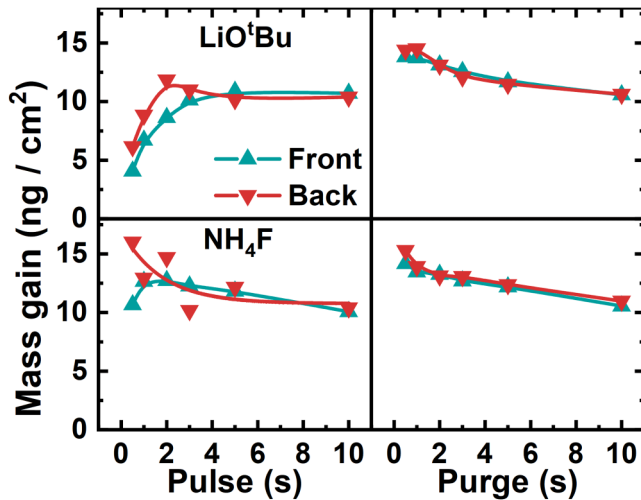


FIG. 2. Mass gain vs pulse and purge parameters investigated by QCM for the  $\text{LiO}^t\text{Bu} + \text{NH}_4\text{F}$  process. All other pulse and purge parameters were kept at 10 s. The deposition temperature was  $225^\circ\text{C}$ . Front and back refer to the placement of the sample in the chamber over 7.5 cm relative to the flow direction. Spline functions are included as a guide for the eye.

We observe a significant mass gain during the  $\text{LiO}^t\text{Bu}$  pulse, followed by an almost as large mass reduction during the  $\text{NH}_4\text{F}$  pulse (Fig. 1). Mass gain per cycle is similar to that reported for the  $\text{LiHMDS} + \text{HF}$ -pyridine process at  $12 \text{ ng/cm}^2$  at  $150^\circ\text{C}$ .<sup>18</sup> Suggested chemical reactions for the  $\text{LiO}^t\text{Bu}$  and  $\text{NH}_4\text{F}$  pulses are summarized in Eqs. (1) and (2). We have used  $\text{NH}_4\text{F}$  as a more safely

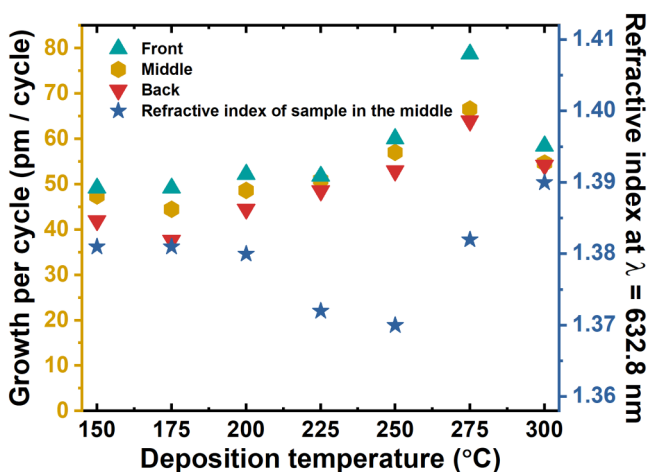


FIG. 3. Growth rate per cycle (left y axis) and refractive index at  $\lambda = 632.8 \text{ nm}$  (right y axis) as a function of deposition temperature for the  $\text{LiO}^t\text{Bu} + \text{NH}_4\text{F}$  process, obtained with spectroscopic ellipsometry. Front, middle, and back refer to the placement of the sample in the chamber over 7.5 cm relative to the flow direction.

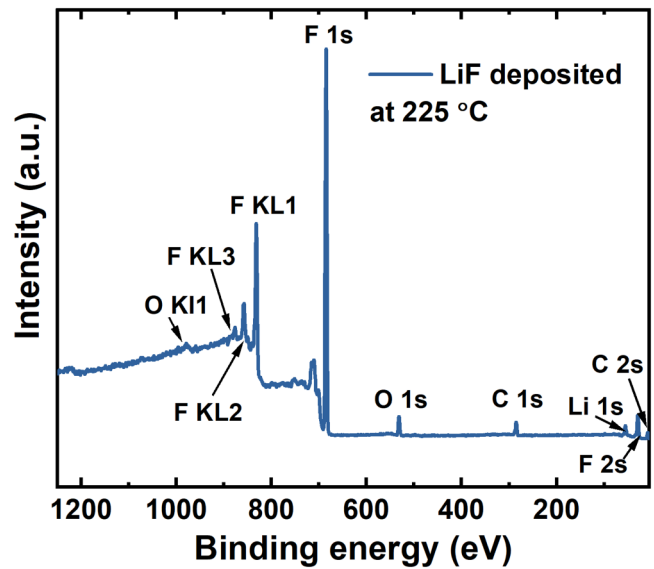
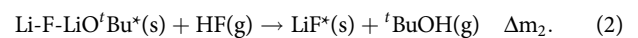


FIG. 4. XPS survey scan of an LiF sample deposited at  $225^\circ\text{C}$ .

manageable source for HF, as  $\text{NH}_4\text{F}$  is known to decompose into  $\text{NH}_3$  and HF upon sublimation. Therefore only HF is considered in the proposed reaction scheme.<sup>19</sup> \* denotes surface species and it should be further noted that LiF is a highly ionic structure where individual charges are distributed over many neighboring atoms,



The net mass gain ratio from one cycle ( $\Delta m_1/\Delta m_2$ ) is 1.45 (Fig. 1). This is in good agreement with the suggested reaction mechanisms [Eqs. (1) and (2)], with a calculated net mass gain ratio of 1.49. Future work, taking advantage of, e.g., *in situ* quadrupole mass spectrometry or similar techniques, could verify that *tert*-butanol is indeed the only by-product of this reaction and also detect  $\text{NH}_3$ .

The  $\text{LiO}^t\text{Bu}$  pulse saturated after about 5 s, and this was used as the pulsing time for  $\text{LiO}^t\text{Bu}$  in further investigations (Fig. 2). A 2 s  $\text{NH}_4\text{F}$  pulse should be sufficient (Fig. 2). In practice, however,

TABLE II. Composition of an LiF sample deposited at  $225^\circ\text{C}$  as measured by XPS.

Compound	Atomic %
Li	52.5
F	40.1
C	4.7
O	2.7



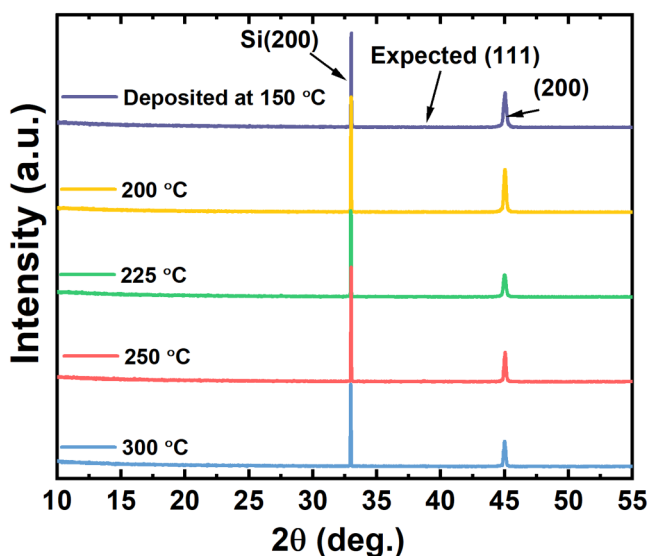


FIG. 5. XRD of LiF thin films deposited at 150, 200, 225, 250, and 300 °C. The (200) reflection from LiF and the Si(200) substrate reflection are marked.

this resulted in large gradients and a 7 s  $\text{NH}_4\text{F}$  pulse was necessary to obtain uniform films.

After establishing pulse and purge parameters for the LiF process, growth per cycle (GPC) and refractive index were investigated as a function of deposition temperature (Fig. 3). The GPC gradually increases with temperature. We believe that the sample at 275 °C follows an increasing trend, while the sample at 300 °C shows deviations resembling initial decomposition or similar. We have several samples deposited at 300 °C confirming the lowered growth rate. The refractive index has a minimum at 250 °C but is close to the reported value of 1.391 at 300 °C, although we see a deviating GPC trend at this temperature.<sup>20</sup> The growth rate of our process is comparable to that of  $\text{LiHMDS} + \text{HF}$ -pyridine and

$\text{LiO}^t\text{Bu} + \text{TiF}_4$  processes, but significantly lower than the rest, where  $\text{LiO}^t\text{Bu} + \text{MoF}_6$  has the highest growth rate at 260 pm per cycle. The low growth rate for our LiF process is not a limitation for its use as surface coating of battery materials, as such films are typically in the subnanometer to the nanometer scale.

Chemical composition and state were further characterized by XPS. Quantification of lithium by XPS is inherently difficult, but a high-resolution survey spectrum was collected to attempt an elemental analysis (Fig. 4 and Table II). See supplementary material<sup>21</sup> for detailed XPS scans. The study points toward the formation of LiF, with a slight over-stoichiometry of lithium. This can be explained by the presence of carbon and oxygen, which is probably present as  $\text{Li}_2\text{CO}_3$ . Using  $\text{LiO}^t\text{Bu}$  is known to result in small amounts of carbon contamination.<sup>22</sup> However, since native SEIs already consist of lithium carbonates,<sup>18</sup> a small amount of  $\text{Li}_2\text{CO}_3$  in the LiF coating is believed to be unproblematic for use in controlling SEI formation. Some of the carbon and oxygen are also believed to stem from  $-\text{C}=\text{O}$  surface species. It is worth noting that that depth analysis is not applicable for lithium-containing films since the etching ions tend to push lithium toward the substrate-film interface. Also take notice that no nitrogen is observed, consistent with the known decomposition of  $\text{NH}_4\text{F}$  into  $\text{NH}_3$  and HF. Time-of-flight elastic recoil detection analysis could, in the future, be used to obtain a depth profile and better understanding of the film composition (including hydrogen).

The crystallinity of the films was investigated by specular XRD (Fig. 5), in addition to synchrotron XRD for reciprocal space mapping, see supplementary material.<sup>21</sup> Specular XRD suggests growth with preferred orientation, whereas the reciprocal space map shows a large in-plane broadening. All investigated films have a (200)-orientation throughout the deposited temperature range (150–300 °C). The expected (111) reflection, which should have around 75% of the intensity of the most intense (200) reflection (COD No. 1831351), is absent. Expected reflections from LiF at a higher  $2\theta$  angle are masked by the Si(100) substrate reflection in the investigated range.

Investigation of the surface morphology with SEM and AFM is not in agreement with a fully oriented sample (Fig. 6). The micrographs reveal a polycrystalline surface consisting of triangular and

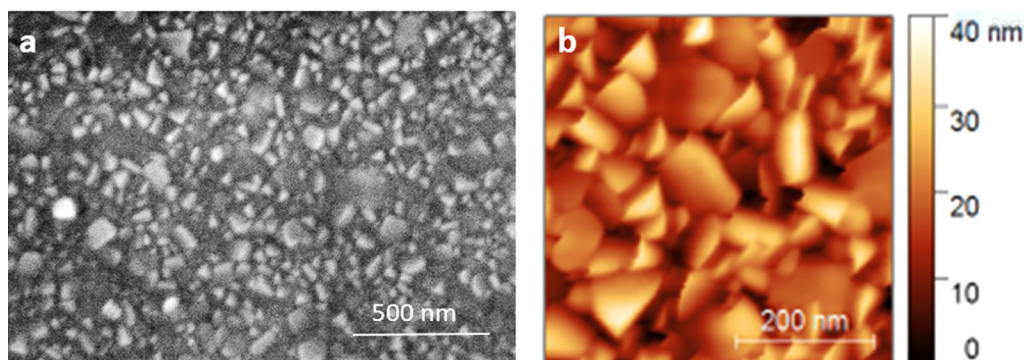


FIG. 6. SEM [(a), left] and AFM [(b), right] micrographs of a 53 nm thick LiF thin film deposited at 225 °C.

square-shaped crystallites, with sizes around 50–100 nm. This is comparable to the film thickness of 53 nm. The RMS roughness is estimated at 6.2 nm from the AFM micrograph. Triangular crystallites correspond to a growth in the (111)-direction, whereas square crystallites correspond to an increase in the (200)-direction.<sup>23</sup>

The lack of the (111)-reflection (Fig. 5) is most likely caused by the low scattering power of LiF.

#### IV. CONCLUSION

In the current work, we show a viable route for deposition of LiF by ALD using LiO<sup>t</sup>Bu and NH<sub>4</sub>F. This process is stable in the temperature range of 150–300 °C, with a GPC of 50.9 pm/cycle and a mass gain per cycle of 10.5 ng/cm<sup>2</sup> cycle at 225 °C. The films are nitrogen-free as measured by XPS but with a possible slight over-stoichiometry of Li and minor carbon contamination. Although conventional Bragg–Brentano and synchrotron XRD suggest (200)-oriented LiF films, both AFM and SEM studies reveal square and triangular crystallites on the surface, indicating random growth.

#### ACKNOWLEDGMENTS

The authors would like to thank the Research Council of Norway for financing this work through the TRALALALA project (No. 244087, Julie N. Kvalvik), RIDSEM project (No. 272253, Henrik H. Sønsteby), Nano-MILIB project (No. 143732, Amund Ruud) and SOLIB project (No. 262387, Kristian B. Kvamme). Moreover, the authors would like to thank Kristian Weibye for assistance with XPS measurements.

#### REFERENCES

<sup>1</sup>E. Ahlswede, J. Hanisch, and M. Powalla, *Appl. Phys. Lett.* **90**, 163504 (2007).  
<sup>2</sup>D. Gao, M. G. Helander, Z.-B. Wang, D. P. Puzzo, M. T. Greiner, and Z.-H. Lu, *Adv. Mater.* **22**, 5404 (2010).  
<sup>3</sup>L. Lu, T. Xu, W. Chen, E. S. Landry, and L. Yu, *Nat. Photonics* **8**, 716 (2014).  
<sup>4</sup>X. Liu, M. Lei, Y. Zhou, B. Song, and Y. Li, *Appl. Phys. Lett.* **107**, 063901 (2015).

<sup>5</sup>J. Seo, S. Park, Y. C. Kim, N. J. Jeon, J. H. Noh, S. C. Yoon, and S. I. Seok, *Energy Environ. Sci.* **7**, 2642 (2014).  
<sup>6</sup>K. Sun, J. Chang, F. H. Isikgor, P. Li, and J. Ouyang, *Nanoscale* **7**, 896 (2015).  
<sup>7</sup>N. Schulz, R. Hausbrand, C. Wittich, L. Dimesso, and W. Jaegermann, *J. Electrochem. Soc.* **165**, A833 (2018).  
<sup>8</sup>P. Verma, P. Maire, and P. Novák, *Electrochim. Acta* **55**, 6332 (2010).  
<sup>9</sup>O. Tiurin, N. Solomatin, M. Auinat, and Y. Ein-Eli, *J. Power Sources* **448**, 227373 (2020).  
<sup>10</sup>Y. S. Jung, A. S. Cavanagh, A. C. Dillon, M. D. Groner, S. M. George, and S.-H. Lee, *J. Electrochem. Soc.* **157**, A75 (2010).  
<sup>11</sup>Y. S. Jung, A. S. Cavanagh, L. A. Riley, S.-H. Kang, A. C. Dillon, M. D. Groner, S. M. George, and S.-H. Lee, *Adv. Mater.* **22**, 2172 (2010).  
<sup>12</sup>H. C. M. Knoops, M. E. Donders, M. C. M. van de Sanden, P. H. L. Notten, and W. M. M. Kessels, *J. Vac. Sci. Technol. A* **30**, 010801 (2012).  
<sup>13</sup>C. Marichy, M. Bechelany, and N. Pinna, *Adv. Mater.* **24**, 1017 (2012).  
<sup>14</sup>C. Zhu, K. Han, D. Geng, H. Ye, and X. Meng, *Electrochim. Acta* **251**, 710 (2017).  
<sup>15</sup>D. M. King, A. Dameron, P. Lichty, and J. Trevey, *Low-Cost Encapsulation of Silicon-Based Nanopowders Final Report* (Forge Nano, Louisville, CO, 2018).  
<sup>16</sup>M. Hossain, K. Khoo, X. Cui, G. Poduval, T. Zhang, X. Li, W. Li, and B. Hoex, “Atomic layer deposition enabling higher efficiency solar cells: A review,” *Nano Mater. Sci.* (in press) (2020).  
<sup>17</sup>M. Ylilammi and T. Ranta-Aho, *J. Electrochem. Soc.* **141**, 1278 (1994).  
<sup>18</sup>L. Younghee, P. Daniela, M. C. Andrew, S. Y. Matthias, J. L. Se-Hee, and G. Steven, “Atomic layer deposition of LiF and lithium ion conducting (AlF<sub>3</sub>) (LiF)<sub>x</sub> alloys using trimethylaluminum, lithium hexamethyldisilazide and hydrogen fluoride,” *ChemRxiv* 12 (2017).  
<sup>19</sup>E. G. Rakov and E. I. Mel’nichenko, *Russ. Chem. Rev.* **53**, 851 (1984).  
<sup>20</sup>H. H. Li, *J. Phys. Chem. Ref. Data* **5**, 329 (1976).  
<sup>21</sup>See supplementary material at <https://doi.org/10.1116/6.0000314> for synchrotron XRD and detailed XPS scans of a LiF film deposited at 225 °C.  
<sup>22</sup>L. Chen *et al.*, *ACS Appl. Mater. Interfaces* **10**, 26972 (2018).  
<sup>23</sup>O. Nilsen, O. B. Karlsen, A. Kjekshus, and H. Fjellvåg, *Thin Solid Films* **515**, 4538 (2007).  
<sup>24</sup>M. Mäntymäki, J. Hämäläinen, E. Puukilainen, F. Munnik, M. Ritala, and M. Leskelä, *Chem. Vap. Deposition* **19**, 111 (2013).  
<sup>25</sup>J. Hennessy and S. Nikzad, *Inorganics* **6**, 46 (2018).  
<sup>26</sup>M. Mäntymäki, M. Ritala, and M. Leskelä, *Coatings* **8**, 227 (2018).  
<sup>27</sup>J. Xie *et al.*, *ACS Nano* **11**, 7019 (2017).